Diffraction by a Parallel-Plate Multiport Using the Method of Kobayashi Potentials

Babak Honarbakhsh*

Faculty of Electrical Engineering, Shahid Beheshti University, 1983963113, Tehran, Iran

e-mail: b_honarbakhsh@sbu.ac.ir

Corresponding author: Babak Honarbakhsh

Phone Number: +98-021-29904192

Mobile: +98-9394431783

Abstract— Application of Kobayashi potentials (KP) is extended to the electromagnetic (EM) diffraction from the parallel-plate multiport. Standard integral identities are used for problem formulation, without the direct use of Weber-Schafheitlin (WS) integrals. The Fourier function space is exploited for the construction of the governing linear system of equations. A simple strategy is suggested for the evaluation of the required improper integrals. Two-dimensional T- and X-junctions are studied as special cases. Numerical results are validated through convergence test and asymptotic analysis. It is shown that whenever the wave number in the whole problem domain is positive, no real power transfers to the diffracted field in the horizontal section of the aforementioned structures.

Keywords —Diffraction, Kobayashi potential, parallel-plate, T-junction, X-junction.

1. INTRODUCTION

THE method of Kobayashi potential (KP) is an interesting semi-analytical method that can handle a

special class of mixed boundary value problems (BVPs) in electromagnetics (EM) [1-3]. In this modal method, by proper application of the Weber-Schafheitlin (WS) integrals, both the edge and the discontinuous Dirichlet boundary conditions (BCs) are automatically satisfied [4]. Hence, providing a unique solution is straightforward. This is in contrast to the modal approach introduced in [5] and the Wiener–Hopf method [6] wherein care should be taken to incorporate the edge condition. Especially, problem formulation by the latter is by no means simple. The KP method can also be considered as a spectral method, wherein the unknown field variable is expanded over a set of WS integrals as basis functions. As a result, the KP method is an excellent candidate to analyze structures with edges and corners and whenever applicable, it would be more efficient than full-wave methods such as the method of moments (MoM) [7] and the finite element method (FEM) [8]. Thus far, the KP method has been applied to specific geometries including flanged waveguides, rectangular strip and crack, and rectangular and circular plates and holes [9-17]. In many related works, the geometry of the structure has remained unchanged, and only the medium is varied [18-27]. Also, the presentation of the method and its numerical implementation is complicated and requires some knowledge of hypergeometric functions and Jacobi's polynomials.

This work extends the class of geometries which can be analyzed using the KP method, by generalizing one the earliest works on this topic [11]. A two-dimensional multiport consisting of an arbitrary number of vertical branches terminating in a common horizontal branch is analyzed. In contrast to almost all papers regarding KP, the method is presented without intricate mathematics. Specifically, some of the special cases of the WS integrals that can be found in standard handbooks are exploited [28]. This eliminates being involved with hypergeometric functions. Also, construction of the governing system of linear equations is performed using the Fourier function space, only [29]. This is in contrast to many related works that use Jacobi's polynomials. Finally, a simple procedure is introduced to evaluate improper integrals, which naturally appears in the KP method. This is also in contrast to similar works wherein rather complicated strategies are suggested. The rest of the paper

is organized as follows: section two is devoted to problem formulation. In section three, the governing equations are derived. Section four describes a method for evaluation of the required integrals. In section five, numerical results are reported. Section six is devoted to a discussion on power flow through the structure. At last, an asymptotic analysis is performed in section seven.

2. STATEMENT OF THE PROBLEM

The cross section of the parallel-plate multiport to be analyzed is depicted in Fig. 1, wherein all the boundaries are perfect electric conductor (PEC). Known EM waves, either TE or TM to x, are incident to vertical branches. It is desired to determine the reflected and diffracted waves in each region. Even-odd decomposition of the total fields leads to [11]:

$$\mathbf{E}^{TE} = \hat{\mathbf{z}}\left(E_0^{TE,e} + E_0^{TE,o}\right) + \hat{\mathbf{z}}\sum_{l=1}^{L}\sum_{n=0}^{\infty}\left(E_{l,n}^{TE,e} + E_{l,n+1}^{TE,o}\right)$$

(1a)

$$\mathbf{H}^{TM} = \hat{\mathbf{z}}\left(H_0^{TM,e} + H_0^{TM,o}\right) + \hat{\mathbf{z}}\sum_{l=1}^{L}\sum_{n=0}^{\infty}\left(H_{l,n}^{TM,e} + H_{l,n}^{TM,o}\right)$$

(1b)

for TE and TM cases, respectively, wherein

$$E_0^{TE,e} = \sum_{l=1}^{L_0}\sum_{n=0}^{\infty} C_{l,n}^{TE}\int_0^{\infty} J_{2n+1}\left(k_x a_l\right)\cos\left[k_x\left(x-x_l\right)\right]\frac{\sin\left[k_y\left(y-d\right)\right]}{k_x\sin\left(k_y d\right)}dk_x$$

$$+\sum_{l=L_0+1}^{L}\sum_{n=0}^{\infty} C_{l,n}^{TE}\int_0^{\infty} J_{2n+1}\left(k_x a_l\right)\cos\left[k_x\left(x-x_l\right)\right]\frac{\sin\left(k_y y\right)}{k_x\sin\left(k_y d\right)}dk_x$$

(2a)

$$E_{l,n}^{TE,e} = \begin{cases} \left[A_{l,2n+1}^{TE}e^{-jh_{l,2n+1}y} + B_{l,2n+1}^{TE}e^{+jh_{l,2n+1}y}\right]\cos\left[\dfrac{(2n+1)\pi}{2a_l}\left(x-x_l\right)\right], & 1<l<L_0 \\ \left[A_{l,2n+1}^{TE}e^{+jh_{l,2n+1}(y-d)} + B_{l,2n+1}^{TE}e^{-jh_{l,2n+1}(y-d)}\right]\cos\left[\dfrac{(2n+1)\pi}{2a_l}\left(x-x_l\right)\right], & L_0+1<l<L \end{cases}$$

(2b)

$$E_0^{TE,o} = \sum_{l=1}^{L_0}\sum_{n=0}^{\infty} D_{l,n}^{TE}\int_0^{\infty} J_{2n+2}\left(k_x a_l\right)\sin\left[k_x\left(x-x_l\right)\right]\frac{\sin\left[k_y\left(y-d\right)\right]}{k_x\sin\left(k_y d\right)}dk_x$$

$$+\sum_{l=L_0+1}^{L}\sum_{n=0}^{\infty} D_{l,n}^{TE}\int_0^{\infty} J_{2n+2}\left(k_x a_l\right)\sin\left[k_x\left(x-x_l\right)\right]\frac{\sin\left(k_y y\right)}{k_x\sin\left(k_y d\right)}dk_x$$

(2c)

$$E_{l,n}^{TE,o} = \begin{cases} \left[A_{l,2n}^{TE}e^{-jh_{l,2n}y} + B_{l,2n}^{TE}e^{+jh_{l,2n}y}\right]\times\sin\left[\dfrac{n\pi}{a_l}\left(x-x_l\right)\right], & 1<l<L_0 \\ \left[A_{l,2n}^{TE}e^{+jh_{l,2n}(y-d)} + B_{l,2n}^{TE}e^{-jh_{l,2n}(y-d)}\right]\times\sin\left[\dfrac{n\pi}{a_l}\left(x-x_l\right)\right], & L_0+1<l<L \end{cases}$$

(2d)

$$H_0^{TM,e} = \sum_{l=1}^{L_0}\sum_{n=0}^{\infty} C_{l,n}^{TM}\int_0^{\infty} J_{2n}\left(k_x a_l\right)\cos\left[k_x\left(x-x_l\right)\right]\frac{\cos\left[k_y\left(y-d\right)\right]}{k_y\sin\left(k_y d\right)}dk_x$$

$$+\sum_{l=L_0+1}^{L}\sum_{n=0}^{\infty} C_{l,n}^{TM}\int_0^{\infty} J_{2n}\left(k_x a_l\right)\cos\left[k_x\left(x-x_l\right)\right]\frac{\cos\left(k_y y\right)}{k_y\sin\left(k_y d\right)}dk_x$$

(2e)

$$H_{l,n}^{TM,e} = \begin{cases} \left[A_{l,2n}^{TM}e^{-jh_{l,2n}y} + B_{l,2n}^{TM}e^{+jh_{l,2n}y}\right]\times\cos\left[\dfrac{n\pi}{a_l}\left(x-x_l\right)\right], & 1<l<L_0 \\ \left[A_{l,2n}^{TM}e^{+jh_{l,2n}(y-d)} + B_{l,2n}^{TM}e^{-jh_{l,2n}(y-d)}\right]\times\cos\left[\dfrac{n\pi}{a_l}\left(x-x_l\right)\right], & L_0+1<l<L \end{cases}$$

(2f)

$$H_0^{TM,o} = \sum_{l=1}^{L_0}\sum_{n=0}^{\infty} D_{l,n}^{TM}\int_0^{\infty} J_{2n+1}\left(k_x a_l\right)\sin\left[k_x\left(x-x_l\right)\right]\frac{\cos\left[k_y\left(y-d\right)\right]}{k_y\sin\left(k_y d\right)}dk_x$$

$$+\sum_{l=L_0+1}^{L}\sum_{n=0}^{\infty} D_{l,n}^{TM}\int_0^{\infty} J_{2n+1}\left(k_x a_l\right)\sin\left[k_x\left(x-x_l\right)\right]\frac{\cos\left(k_y y\right)}{k_y\sin\left(k_y d\right)}dk_x$$

(2g)

$$H_{l,n}^{TM,o}=\begin{cases}\left[A_{l,2n+1}^{TM}e^{-jh_{l,2n+1}y}+B_{l,2n+1}^{TM}e^{+jh_{l,2n+1}y}\right]\times\sin\left[\dfrac{(2n+1)\pi}{2a_l}(x-x_l)\right], & 1<l<L_0\\ \left[A_{l,2n+1}^{TM}e^{+jh_{l,2n+1}(y-d)}+B_{l,2n+1}^{TM}e^{-jh_{l,2n+1}(y-d)}\right]\times\sin\left[\dfrac{(2n+1)\pi}{2a_l}(x-x_l)\right], & L_0+1<l<L\end{cases}$$

(2h)

In (2) and according to Fig. 1, A_α^β 's are known and represent the amplitude of incident waves. The rest of the constants are to be determined which denote amplitudes of reflected waves (B_α^β's) and diffracted fields (C_α^β 's and D_α^β 's). In addition,

$k_x^2+k_y^2=k_l^2,\ l=0$

(3a)

$h_{l,n}^2=k_l^2-\left(n\pi/2a_l\right)^2,\ \mathrm{Im}\left\{h_{l,n}\right\}<0,\ l\neq 0$

(3b)

with $k_l^2=\omega^2\mu_l\varepsilon_l$. The condition on the imaginary part of $h_{l,n}$ ensures that reflected waves satisfy the Sommerfeld radiation condition at infinity. However, both values of k_y are valid since corresponding expressions are even functions of k_y. It is worth noting that all auxiliary conditions governing the problem, including null tangential electric field over the conducting boundaries and the required edge conditions, are automatically satisfied by virtue of a particular class of WS integrals (Appendix A) as represented by (2a), (2c), (2e), and (2g). The unknown constants can be computed by imposing the continuity of tangential EM fields at the junctions. In the KP method, this step is often carried out by limiting the number of modes to a finite number (*N*), expanding the fields over a suitable function space, and finally, solving the resulting linear system of equations. The formulation can be extended to incorporate a line source excitations that is a 2D analogue to the coaxial probe feed [11]. In addition, based on [16], extension to a rectangular waveguide multiport is, also, possible.

3. DERIVING THE GOVERNING EQUATIONS

In this paper, all the resulting equations obtained from the imposition of continuity conditions are expanded over the Fourier function space (Appendix B). This approach is simple and efficient since it does not require being involved with Jacobi's polynomials and hypergeometric functions. As well, Bessel function evaluations reduce and some of the resulting matrices diagonalize. Finally, assuming ξ as the integration variable, the integrands decay with $\xi^{5/2}$ that is $\xi^{1/2}$ order faster compared to those obtained using the Bessel function space. Specifically, when using Bessel function space, the integrand includes the product of two Bessel functions, each with the decaying rate of $\xi^{-1/2}$, and a function with the decaying rate of ξ^{-1} [11]. On the other hand, when using Fourier function space, one of the Bessel functions becomes substituted by a rational function with a decaying rate of ξ^{-2}.

3.1. TE case

For TE-mode wave incidence, governing equations to unknown constants are:

$$A_{l,2n+1}^{TE}+B_{l,2n+1}^{TE}=\frac{-2}{2n+1}\sum_{m=0}^{N-1}C_{l,m}^{TE}J_{2m+1}\left(\frac{(2n+1)\pi}{2}\right),\quad 0<l\le L_0$$

(4a)

$$A_{l,2n+1}^{TE}+B_{l,2n+1}^{TE}=\frac{+2}{2n+1}\sum_{m=0}^{N-1}C_{l,m}^{TE}J_{2m+1}\left(\frac{(2n+1)\pi}{2}\right),\quad L_0<l\le L$$

(4b)

$$\frac{\mu_r^0}{j\mu_r^l}\left(A_{l,2n+1}^{TE}-B_{l,2n+1}^{TE}\right)h_{l,2n+1}=\sum_{l=1}^{L_0}\sum_{m=0}^{N-1}C_{l,m}^{TE}P_{l,e}^{TE}(m,n)+\sum_{l=L_0+1}^{L}\sum_{m=0}^{N-1}C_{l,m}^{TE}Q_{l,e}^{TE}(m,n),\quad 0<l\le L_0$$

(4c)

$$\frac{j\mu_r^0}{\mu_r^l}\left(A_{l,2n+1}^{TE}-B_{l,2n+1}^{TE}\right)h_{l,2n+1}=\sum_{l=1}^{L_0}\sum_{m=0}^{N-1}C_{l,m}^{TE}Q_{l,e}^{TE}(m,n)+\sum_{l=L_0+1}^{L}\sum_{m=0}^{N-1}C_{l,m}^{TE}P_{l,e}^{TE}(m,n),\quad L_0<l\le L$$

(4d)

$$A_{l,2n}^{TE}+B_{l,2n}^{TE}=\frac{-1}{n}\sum_{m=0}^{N-1}D_{l,m}^{TE}J_{2m+2}\left(n\pi\right),\quad 0<l\le L_0$$

(4e)

$$A_{l,2n}^{TE}+B_{l,2n}^{TE}=\frac{+1}{n}\sum_{m=0}^{N-1}D_{l,m}^{TE}J_{2m+2}\left(n\pi\right),\quad L_0<l\le L$$

(4f)

$$\frac{j\mu_r^0}{\mu_r^l}\left(A_{l,2n}^{TE}-B_{l,2n}^{TE}\right)h_{l,2n}=\sum_{l=1}^{L_0}\sum_{m=0}^{N-1}D_{l,m}^{TE}P_{l,o}^{TE}\left(m,n\right)+\sum_{l=L_0+1}^{L}\sum_{m=0}^{N-1}D_{l,m}^{TE}Q_{l,o}^{TE}\left(m,n\right),\quad 0<l\le L_0$$

(4g)

$$\frac{\mu_r^0}{j\mu_r^l}\left(A_{l,2n}^{TE}-B_{l,2n}^{TE}\right)h_{l,2n}=\sum_{l=1}^{L_0}\sum_{m=0}^{N-1}D_{l,m}^{TE}Q_{l,o}^{TE}\left(m,n\right)+\sum_{l=L_0+1}^{L}\sum_{m=0}^{N-1}D_{l,m}^{TE}P_{l,e}^{TE}\left(m,n\right),\quad L_0<l\le L$$

(4h)

where μ_r^l denotes relative magnetic permeability of R_l and

$$P_{l,e}^{TE}\left(m,n\right)=\left(-1\right)^n\left(2n+1\right)\pi\times\mathbf{p.v.}\int_0^\infty\frac{J_{2m+1}\left(k_xa_l\right)\cos\left(k_xa_l\right)}{\left[\left(2n+1\right)\pi/2\right]^2-\left(k_xa_l\right)^2}k_y\cot\left(k_yd\right)k_x^{-1}dk_x \tag{5a}$$

$$Q_{l,e}^{TE}\left(m,n\right)=\left(-1\right)^n\left(2n+1\right)\pi\times\mathbf{p.v.}\int_0^\infty\frac{J_{2m+1}\left(k_xa_l\right)\cos\left(k_xa_l\right)}{\left[\left(2n+1\right)\pi/2\right]^2-\left(k_xa_l\right)^2}k_y\csc\left(k_yd\right)k_x^{-1}dk_x \tag{5b}$$

$$P_{l,o}^{TE}\left(m,n\right)=\left(-1\right)^n\left(2\pi\right)\times\mathbf{p.v.}\int_0^\infty\frac{J_{2m+2}\left(k_xa_l\right)\sin\left(k_xa_l\right)}{\left(k_xa_l\right)^2-\left(n\pi\right)^2}k_y\cot\left(k_yd\right)k_x^{-1}dk_x \tag{5c}$$

$$Q_{l,o}^{TE}\left(m,n\right)=\left(-1\right)^n\left(2\pi\right)\times\mathbf{p.v.}\int_0^\infty\frac{J_{2m+2}\left(k_xa_l\right)\sin\left(k_xa_l\right)}{\left(k_xa_l\right)^2-\left(n\pi\right)^2}k_y\csc\left(k_yd\right)k_x^{-1}dk_x \tag{5d}$$

In (5), the "**p.v.**" stands for the *Cauchy principal value* to consider singularities of the integrands. Eq. (4) contains $4L$ equations, each of them is an $N\times N$ linear system and can be efficiently solved for the unknowns. Note that all matrices corresponding to the left-hand side of (4) are diagonal. This is not the case when the Bessel function space is used.

3.2. TM case

For TM-mode wave incidence, governing equations to unknown constants are:

$$\frac{\left(1+\delta_{0n}\right)h_{l,2n}\varepsilon_r^0}{j\varepsilon_r^l}\left(A_{l,2n}^{TM}-B_{l,2n}^{TM}\right)=\sum_{m=0}^{N-1}C_{l,m}^{TM}J_{2m}\left(n\pi\right),\quad 0<l\le L_0$$

(6a)

$$\frac{j\left(1+\delta_{0n}\right)h_{l,2n}\varepsilon_r^0}{\varepsilon_r^l}\left(A_{l,2n}^{TM}-B_{l,2n}^{TM}\right)=\sum_{m=0}^{N-1}C_{l,m}^{TM}J_{2m}\left(n\pi\right),\quad L_0<l\le L$$

(6b)

$$\left(1+\delta_{0n}\right)\left(A_{l,2n}^{TM}+B_{l,2n}^{TM}\right)=\sum_{l=1}^{L_0}\sum_{m=0}^{N-1}C_{l,m}^{TM}P_{l,e}^{TM}\left(m,n\right)+\sum_{l=L_0+1}^{L}\sum_{m=0}^{N-1}C_{l,m}^{TM}Q_{l,e}^{TM}\left(m,n\right),\quad 0<l\le L_0$$

(6c)

$$\left(1+\delta_{0n}\right)\left(A_{l,2n}^{TM}+B_{l,2n}^{TM}\right)=\sum_{l=1}^{L_0}\sum_{m=0}^{N-1}C_{l,m}^{TM}Q_{l,e}^{TM}\left(m,n\right)+\sum_{l=L_0+1}^{L}\sum_{m=0}^{N-1}Q_{l,m}^{TM}Q_{l,e}^{TM}\left(m,n\right),\quad 0<l\le L_0$$

(6d)

$$\left(A_{l,2n+1}^{TM}-B_{l,2n+1}^{TM}\right)=\sum_{m=0}^{N-1}D_{l,m}^{TM}J_{2m+1}\left(\frac{\left(2n+1\right)\pi}{2}\right),\quad 0<l\le L_0$$

(6e)

$$\frac{jh_{l,2n+1}\varepsilon_r^0}{\varepsilon_r^l}\left(A_{l,2n+1}^{TM}-B_{l,2n+1}^{TM}\right)=\sum_{m=0}^{N-1}D_{l,m}^{TM}J_{2m+1}\left(\frac{\left(2n+1\right)\pi}{2}\right),\quad L_0<l\le L$$

(6f)

$$A_{l,2n+1}^{TE}+B_{l,2n+1}^{TE}=\sum_{l=1}^{L_0}\sum_{m=0}^{N-1}D_{l,m}^{TM}P_{l,o}^{TM}\left(m,n\right)+\sum_{l=L_0+1}^{L}\sum_{m=0}^{N-1}D_{l,m}^{TE}Q_{l,o}^{TM}\left(m,n\right),\quad 0<l\le L_0$$

(6g)

$$A_{l,2n}^{TE}+B_{l,2n}^{TE}=\sum_{l=1}^{L_0}\sum_{m=0}^{N-1}D_{l,m}^{TM}Q_{l,o}^{TM}\left(m,n\right)+\sum_{l=L_0+1}^{L}\sum_{m=0}^{N-1}D_{l,m}^{TM}P_{l,e}^{TM}\left(m,n\right),\quad L_0<l\le L$$

(6h)

where ε_r^l denotes relative electric permittivity of R_l and

$$P_{l,e}^{TM}\left(m,n\right)=2\left(-1\right)^{n}\times\mathbf{p.v.}\int_{0}^{\infty}\frac{J_{2m}\left(k_{x}a_{l}\right)\sin\left(k_{x}a_{l}\right)}{\left(k_{x}a_{l}\right)^{2}-\left(n\pi\right)^{2}}k_{y}^{-1}\cot\left(k_{y}d\right)k_{x}dk_{x} \tag{7a}$$

$$Q_{l,e}^{TM}\left(m,n\right)=2\left(-1\right)^{n}\times\mathbf{p.v.}\int_{0}^{\infty}\frac{J_{2m}\left(k_{x}a_{l}\right)\sin\left(k_{x}a_{l}\right)}{\left(k_{x}a_{l}\right)^{2}-\left(n\pi\right)^{2}}k_{y}^{-1}\csc\left(k_{y}d\right)k_{x}dk_{x} \tag{7b}$$

$$P_{l,o}^{TM}\left(m,n\right)=2\left(-1\right)^{n}\times\mathbf{p.v.}\int_{0}^{\infty}\frac{J_{2m}\left(k_{x}a_{l}\right)\cos\left(k_{x}a_{l}\right)}{\left(n\pi/2\right)^{2}-\left(k_{x}a_{l}\right)^{2}}k_{y}^{-1}\cot\left(k_{y}d\right)k_{x}dk_{x} \tag{7c}$$

$$Q_{l,o}^{TM}\left(m,n\right)=2\left(-1\right)^{n}\times\mathbf{p.v.}\int_{0}^{\infty}\frac{J_{2m}\left(k_{x}a_{l}\right)\cos\left(k_{x}a_{l}\right)}{\left(n\pi/2\right)^{2}-\left(k_{x}a_{l}\right)^{2}}k_{y}^{-1}\csc\left(k_{y}d\right)k_{x}dk_{x}. \tag{7d}$$

4. EVALUATION OF INTEGRALS

Each of the TE and TM wave incidences leads to four sets of integrals with similar mathematical structures. For brevity, two set for each case is studied here. Also, multiplicative constants are neglected. It is assumed that the wave number in the whole problem domain is a positive value.

4.1. TE case

Consider the semi-infinite integral of the form:

$$I_{\alpha}^{TE}=\mathbf{p.v.}\int_{0}^{\infty}f_{\alpha}^{TE}\left(\xi\right)d\xi,\qquad f_{\alpha}^{TE}=g_{J}^{TE}g_{c}^{TE}g_{\alpha}^{TE} \tag{8}$$

wherein

$$g_{J}^{TE}\left(\xi\right)=\xi^{-1}J_{2m+1}\left(\xi\right),\qquad m=0,1,2,\ldots \tag{9a}$$

$$g_{c}^{TE}\left(\xi\right)=\frac{\cos\xi}{\xi^{2}-\left[\left(2n+1\right)\pi/2\right]^{2}},\qquad n=0,1,2,\ldots \tag{9b}$$

$$g_{\alpha}^{TE}(\xi)=\begin{cases}\kappa_y \cot\left(\kappa_y d_0\right), & \alpha = b \\ \kappa_y \csc\left(\kappa_y d_0\right), & \alpha = u\end{cases}$$

(9c)

Note that g_J^{TE} and g_c^{TE} are undefined at $\xi = 0,(2n+1)\pi/2$. Since $J_\nu(x)$ is zero at the origin, the singularity of the former is removable. By applying L'Hopital's rule, it can be seen that singularities of g_c^{TE} are also removable and $\left|g_c^{TE}\right| \le 1/2$. Thus, singularities of (9) are not troublesome. To numerically evaluate (8), the corresponding integral is partitioned at the branch-point singularity of g_{α}^{TE} to $I_{\alpha,1}^{TE}$, $I_{\alpha,2}^{TE}$ and $I_{\alpha,3}^{TE}$, defined by:

$$I_{\alpha,1}^{TE} = \mathbf{p.v.}\int_0^{\kappa_2} g_J^{TE}(\xi)\, g_c^{TE}(\xi)\, g_{\alpha,1}^{TE}(\xi)\, d\xi$$

(10a)

$$I_{\alpha,2}^{TE} = \mathbf{p.v.}\int_{\kappa_2}^{\kappa_\alpha^{TE}} g_J^{TE}(\xi)\, g_c^{TE}(\xi)\, g_{\alpha,2}^{TE}(\xi)\, d\xi$$

(10b)

$$I_{\alpha,3}^{TE} = \mathbf{p.v.}\int_{\kappa_\alpha^{TE}}^{\infty} g_J^{TE}(\xi)\, g_c^{TE}(\xi)\, g_{\alpha,2}^{TE}(\xi)\, d\xi$$

(10c)

with

$$g_{\alpha,1}^{TE}(\xi)=\begin{cases}\sqrt[+]{\kappa_2^2-\xi^2}\cot\left(d_0\sqrt[+]{\kappa_2^2-\xi^2}\right), & \alpha = b \\ \sqrt[+]{\kappa_2^2-\xi^2}\csc\left(d_0\sqrt[+]{\kappa_2^2-\xi^2}\right), & \alpha = u\end{cases}$$

(11a)

$$g_{\alpha,2}^{TE}(\xi)=\begin{cases}\sqrt[+]{\xi^2-\kappa_2^2}\coth\left(d_0\sqrt[+]{\xi^2-\kappa_2^2}\right), & \alpha = b \\ \sqrt[+]{\xi^2-\kappa_2^2}\operatorname{csch}\left(d_0\sqrt[+]{\xi^2-\kappa_2^2}\right), & \alpha = u\end{cases}$$

(11b)

where the plus sign over the square root indicates its principal branch to ensure satisfying the radiation condition. The value of κ_α^{TE} is not determined, yet. Again, using L'Hopital's rule it can be seen that all singularities of $g_{\alpha,1}^{TE}$ are removable. Due to the periodicity of the trigonometric functions, *i.e.*, cotangent and cosecant, the number of such points may be more than one. On the other hand, the (real) hyperbolic functions have only one singularity at their center of symmetry which in the present case, removes by the corresponding coefficient functions. As a result, standard quadrature rules can handle evaluation of $I_{\alpha,1}^{TE}$ and $I_{\alpha,2}^{TE}$. The remained task is to find a proper value for κ_α^{TE} and to develop a method to properly approximate $I_{\alpha,3}^{TE}$; *i.e.*, the integral tail. For this purpose, note that hyperbolic functions are positive and monotonically decreasing when $\xi > \kappa_2$ with the limiting value of unity for hyperbolic cotangent and zero for hyperbolic cosecant. Also, it is well known that $\left|J_\nu\left(x\right)\right| \le 1$ for real arguments [30]. Thus,

$$\left|I_{\alpha,2}^{TE}\right| \le \begin{cases} \displaystyle\int_{v_2^{TE}}^{v_b^{TE}} \frac{1}{d_0} \frac{\coth v}{\left|\left(v/d_0\right)^2 + \kappa_2^2 - \left[\left(2n+1\right)\pi/2\right]^2\right|} \frac{v}{\sqrt[+]{v^2 + \left(d_0\kappa_2\right)^2}}\, dv, \ \alpha = b \\ \displaystyle\int_{v_2^{TE}}^{v_u^{TE}} \frac{1}{d_0} \frac{\operatorname{csch} v}{\left|\left(v/d_0\right)^2 + \kappa_2^2 - \left[\left(2n+1\right)\pi/2\right]^2\right|} \frac{v}{\sqrt[+]{v^2 + \left(d_0\kappa_2\right)^2}}\, dv, \ \alpha = u \end{cases}$$

(12)

where $v = d_0\sqrt{\xi^2 - \kappa_2^2}$ with the corresponding integration limits. The "**p.v.**" symbol is omitted since, as discussed, singularities of the integrand can be removed. Let the below conditions meet:

$$\left(v_\alpha^{TE}/d_0\right)^2 + \kappa_2^2 > \left[\left(2n+1\right)\pi/2\right]^2$$

(13a)

$$\coth v_b^{TE} < 1 + 10^{-p_b^{TE}}$$

(13b)

$$\operatorname{csch} v_u^{TE} < 1 + 10^{-p_u^{TE}}$$

(13c)

where p_α^{TE} is a positive control parameter. Then, the integrand of $I_{\alpha,3}^{TE}$ becomes a monotonically decreasing function. Additionally, a sufficiently large p_α^{TE} ensures that v_α^{TE} is far from branch-point of the hyperbolic functions and consequently those can be replaced by their limiting value at infinity leading to $I_{u,3}^{TE} \cong 0$. Nevertheless, a very large p_α^{TE} leads to a long tail that makes the numerical integration difficult and time-consuming. In the present work, by trial and error, the said control parameters are set equal to two. This completes determination of κ_α^{TE}.To evaluated $I_{b,3}^{TE}$, the Bessel function in the corresponding integrand is replaced by its large-argument approximation [30]:

$$J_{2m+1}(\xi) \cong \sqrt{2/\pi\xi}\cos\left(\xi - (2m+1)\pi/2 - \pi/4\right)$$

(14)

leading to

$$f_b^{TE}(\xi) = \frac{(-1)^m}{j2\sqrt{\pi}} f_o^{TE}(\xi) f_d^{TE}(\xi)$$

(15)

for $\xi \in \left(\kappa^{TE}, \infty\right)$, where

$$f_o^{TE}(\xi) = -1 + \sin 2\xi + \cos 2\xi$$

(16a)

$$f_d^{TE}(\xi) = \frac{\xi^{-3/2}\left(\xi^2 - \kappa_2^2\right)^{1/2}}{\xi^2 - \left[(2n+1)\pi/2\right]^2}$$

(16b)

Applying the Binomial expansion to (16b) results in

$$f_d^{TE}(\xi) \cong \xi^{-5/2}\left(1-\kappa_2^2/2\xi^2\right)\left(1+\left[(2n+1)\pi/2\right]^2/\xi^2\right)$$

(17)

which has a known antiderivative. Noting (16a) and inspired by the Riemann-Lebesgue lemma [31], $I_{b,3}^{TE}$ can be approximated by,

$$I_{b,3}^{TE} \cong \frac{(-1)^{m+1}}{j2\sqrt{\pi}} \int_{\kappa_b^{TE}}^{\infty} f_d^{TE}(\xi)$$

(18)

which can be computed analytically.

4.2. TM case

Consider the semi-infinite integral of the form:

$$I_\alpha^{TM} = \mathbf{p.v.}\int_0^\infty f_\alpha^{TM}(\xi)\,d\xi, \qquad f_\alpha^{TM} = g_J^{TM} g_c^{TM} g_\alpha^{TM}$$

(19)

wherein:

$$g_J^{TM}(\xi) = J_{2m}(\xi), \qquad m = 0,1,2,\ldots$$

(20a)

$$g_c^{TM}(\xi) = \frac{\xi \sin\xi}{\xi^2 - (n\pi)^2}, \qquad n = 0,1,2,\ldots$$

(20b)

$$g_\alpha^{TM}(\xi) = \kappa_y^{-1} \cot(\kappa_y d_0)$$

(20c)

Similar to the previous case, there is no concern with g_J^{TM} and g_c^{TM}. Additionally, it can be seen that $\left|g_c^{TM}\right| \le 1/2$ which occurs at $\xi = n\pi$. To numerically evaluate (19), the corresponding integral is

partitioned at the branch- point singularity of g_{α}^{TE} to $I_{\alpha,1}^{TE}$, $I_{\alpha,2}^{TE}$ and $I_{\alpha,3}^{TE}$, defined by:

$$I_{\alpha,1}^{TM} = \mathbf{p.v.}\int_0^{\kappa_2} g_J^{TM}(\xi)\, g_c^{TM}(\xi)\, g_{\alpha,1}^{TM}(\xi)\, d\xi$$

(21a)

$$I_{\alpha,2}^{TM} = \mathbf{p.v.}\int_{\kappa_2}^{\kappa_\alpha^{TM}} g_J^{TM}(\xi)\, g_c^{TM}(\xi)\, g_{\alpha,2}^{TM}(\xi)\, d\xi$$

(21b)

$$I_{\alpha,3}^{TM} = \mathbf{p.v.}\int_{\kappa_\alpha^{TM}}^{\infty} g_J^{TM}(\xi)\, g_c^{TM}(\xi)\, g_{\alpha,2}^{TM}(\xi)\, d\xi \qquad (21c)$$

with

$$g_{\alpha,1}^{TE}(\xi) = \begin{cases} \cot\left(d_0 \sqrt[+]{\kappa_2^2 - \xi^2}\right) / \sqrt[+]{\kappa_2^2 - \xi^2}, & \alpha = b \\ \csc\left(d_0 \sqrt[+]{\kappa_2^2 - \xi^2}\right) / \sqrt[+]{\kappa_2^2 - \xi^2}, & \alpha = u \end{cases}$$

(22a)

$$g_{\alpha,2}^{TE}(\xi) = \begin{cases} \coth\left(d_0 \sqrt[+]{\xi^2 - \kappa_2^2}\right) / \sqrt[+]{\xi^2 - \kappa_2^2}, & \alpha = b \\ \operatorname{csch}\left(d_0 \sqrt[+]{\xi^2 - \kappa_2^2}\right) / \sqrt[+]{\xi^2 - \kappa_2^2}, & \alpha = u \end{cases}$$

(22b)

The value of κ_α^{TM} is to be determined. In contrast to the TE case, singularities of $g_{\alpha,1}^{TE}$ and $g_{\alpha,2}^{TE}$ are not removable and thus, the integrand of (19) is not Riemann integrable. Nevertheless, since all of the involved trigonometric and hyperbolic functions have odd symmetry about their branch points, the Cauchy principal value of (19) exists. For numerical implementation, a small neighborhood around such singularities is eliminated from the integration domain. Theoretically, the value for the radii of the excluded domains must approach zero, which its numerical implementation is not possible. Yet, a suitable small value can be considered to neither perturb the convergence of numerical quadrature nor the final solution. Here, by trial and error, this value is found to be $10^{-2}\kappa_2$. Similar to the TE case,

a proper value for κ_α^{TM} satisfies the below conditions:

$$\left(v_\alpha^{TM}/d_0\right)^2+\kappa_2^2>\left(n\pi\right)^2 \tag{23a}$$

$$\coth v_b^{TM}<1+10^{-p_b^{TM}} \tag{23b}$$

$$\operatorname{csch} v_u^{TM}<1+10^{-p_u^{TM}} \tag{23c}$$

where p_α^{TM} is a positive control parameter leading to, $I_{u,3}^{TM}\cong 0$. Additionally, it is straightforward to show that

$$I_3^{TM}\cong\frac{(-1)^m}{j2\sqrt{\pi}}\int_{\kappa_b^{TM}}^{\infty} f_d^{TM}(\xi) \tag{24}$$

where

$$f_d^{TM}(\xi)\cong\xi^{-5/2}\left(1-\kappa_2^2/2\xi^2\right)\left(1+\left(n\pi\right)^2/\xi^2\right). \tag{25}$$

5. NUMERICAL RESULTS

In this section, numerical results regarding to two special cases of the parallel-plate multiport are reported; *i.e.*, air-filled parallel-pate T- and X-junctions. For each case, the structure is excited from the bottom vertical branch by the first mode for each polarization; *i.e.*,

$$\mathbf{E}_i^{TE}=\hat{\mathbf{z}}\cos\left(\pi x/2a\right) \tag{26a}$$

$$\mathbf{H}_i^{TM}=\hat{\mathbf{z}} \tag{26b}$$

wherein a denotes the width of the vertical branch. It is assumed that $\kappa a = 4$ and $\kappa d = 10$ to ensure the applicability of the method and validity of formulation for relatively large structures. Numerical integrations are performed using MATLAB® integral function which can, automatically, handle weak singularities. Validation is carried out based on the convergence analysis [32]. The second norm of the electric (magnetic) field over the junction is used as the convergence measure for TE (TM) polarization. All magnitude distributions are normalized to the corresponding maximum value. For clarity, magnitudes of surface field distributions are reported on the logarithmic scale. Curves including the CPU time are not included for brevity. To provide an estimate for computational cost, analysis with 4 modes lasts about 0.2 seconds. Simulations has been accomplished using a personal computer with an Intel® Core™ i7-4790K processor.

Based on Fig. 2, two-digit precision achieves with three modes and thus, the method is fast converging. Representative singular fields over the junctions are reported in Figs. 3 and 4 which validates the satisfying of continuity and edge conditions over the junctions [33]. In the aforementioned figures, mag. and ang. stands for, respectively, magnitude (in the corresponding unit) and angle (in radians). Note that singular fields are better followed in the horizontal section due to the presence of a continuous spectrum of eigenvalues in the WS integrals. Based on the results above, it can be claimed that the solutions are valid. Lastly, surface field distributions are reported in Figs. 5 to 8. In the T-junction, the diffracted field is transmissive-like in the horizontal branch. However, as will be discussed in the next section, there is no transmission of energy. This fact is verified numerically but not reported due to almost null field distributions. In the X-junction, note how the field pattern in the vertical branches changes after passing through the junction due to EM diffraction.

6. DISCUSSION

As mentioned in the previous section, despite what appears from the graphical representation of the reported field distributions, there is no energy transfer in the T-junction. Here, this fact is justified for the TM case. A similar analysis can be performed for the TE case. Again, it is assumed that the wave number in the whole problem domain is positive. Therefore, the manner in which EM fields are represented in section two is in accordance with the said situation, since field variation in both the longitudinal and transverse directions become sinusoidal, leading to standing waves in both dimensions. Furthermore, the magnetic field in the region (2) can be, equivalently, expressed as:

$$H_z^{(2)}(x,y) = H_z^{(2+)}(x,y) + H_z^{(2-)}(x,y)$$

(27)

where

$$H_z^{(2\pm)}(x,y) = \int_0^{\infty} V^{\pm}(k_x) \frac{\cos\left[k_y(y-d)\right]}{k_y \sin(k_y d)} e^{\mp jk_x x} dk_x$$

(28)

are, respectively, forward and backward traveling waves in the x direction. It is simple to show that:

$$V^{\pm}(k_x) = \frac{1}{2}\sum_{m=0}^{\infty}\left[C_m J_{2m}(k_x a) \pm jD_m J_{2m+1}(k_x a)\right]$$

(29)

Consequently, exciting a pure traveling wave in either of the longitudinal directions requires C_m and D_m to be proportional; *i.e.*, removing either forward or backward waves, necessitates $C_m = \pm jD_m J_{2m+1}(k_x a)/J_{2m}(k_x a)$. This eliminates one degree of freedom in the solution step and prohibits the imposition of the continuity condition at the junction. One may wonder since the incident power from the vertical section cannot enter to the horizontal part, irrespective to the dimensions of the structure. Numerical study of the T-junction shows that the incident power is

either zero $\left(ak_1 < \pi/2\right)$ or totally reflects $\left(ak_1 > \pi/2\right)$. The former can be concluded by noting (2f) and (2h) and is valid for the X-junction, also. At the first look, this result is in contradiction with various works on the parallel-plate T-junction which confirm real power transfer between its different branches [34-39]. It is worth noting that there are two fundamental differences between those works and the present solution. In none of the above-mentioned works, the edge condition has been discussed. As well, in the above-mentioned papers, the T-junction has been viewed as a microwave component with an emphasis on power transmission and the problem has been solved for EM modes containing a pure traveling wave in the vertical branch. On the contrary, here, EM diffraction is studied, without any matching constraint. Thus, previous and present solutions differ in the sense of EM modes which the problem is solved for. Note that the S-parameter measurement which has been validated in the aforementioned works defines under matched conditions [40]. Especially, [39] has validated analytical results of [35] using the finite-difference finite-frequency (FDFD) method wherein perfectly matched layer absorbing boundary conditions are used at all boundaries. This is equivalent to terminate the branches of the structure by matched loads. Nonetheless, in the KP method, imposing any additional condition in the longitudinal direction is equivalent to changing the functional form of the sine or cosine argument in the WS integrals, which destroys the edge condition at the desired location. Thus, as long as the wave number in the whole problem domain is positive and, as long as considering the edge condition is of interest and, as long as the branches of the T-junction are of an infinite extend and, as long as no matching condition is imposed, there is no real power transfer from the vertical section to the horizontal part. The above-mentioned situation can be verified by considering power flow in the X-junction which shows that a part of the incident wave to the lower section of the vertical branch reflects and the rest of it enters the upper one (Fig. 9).

As the final note, since the KP method is based on modal expansion, its efficiency decreases as the

junction width increases due to a large number of modes which is required for the construction of the solution. The aforementioned shortcoming mainly stems from numerical error concerning the evaluation of the required integrals, which leads to a slower convergence rate and an increase in computational cost (Fig. 10). It is well-known that in such situations, either full-wave or high-frequency methods are wise choices for performing EM analysis.

7. ASYMPTOTIC ANALYSIS

To the best of the knowledge of the author, no solution to the problem at hand is reported yet, either analytical or numerical. Especially, no commercial software is capable to solve the problem, mainly due to its infinite extent in both dimensions and no matching constrain. Yet, in two limiting cases, the solution of the T-junction is known by which the presented method can be further validated. Specifically, when $d = 0$, the structure becomes a short-circuited parallel-plate waveguide leading to zero boundary electric field, and when $d = \infty$, it becomes a flanged parallel-plate waveguide which has a semi-analytical solution [11]. Fig. 11 demonstrates how the KP results approach to the known solutions for the TE case, wherein $d = \infty$ corresponds to the KP solution for the flanged parallel-plate waveguide. When $d = \infty$, it is assumed that $k_y = k_y^{'} - jk_y^{''}$ with positive $k_y^{'}$ and $k_y^{''}$ to satisfy the radiation condition at $y = +\infty$. Regarding the complex k_y are two points to be mentioned. First, the evaluation of the required integrals simplifies due to shifting the singularities of the cotangent function from the real axis into the complex plane. Second, in this case, real power transfers into the diffracted field. The same analysis can be performed for the TM case, which is not included for brevity.

8. COMPARISON WITH ANALYTICAL SERIES SOLUTION

It would be informative to compare the KP solution with another analytical solution for the problem at hand. For this purpose, the analytical series solution (SS) developed in [35] and [36] is selected,

and the corresponding results are reported in Figs. 12 and 13 for TE and TM polarization, respectively. It should be noted that the SS method does not consider the edge condition. The result of such a lack can be clearly seen in Fig. 12(b) and Fig. 13(a) wherein the singular component of the EM field over the aperture is demonstrated. Specifically, the SS prediction is incapable of tracking the corresponding singularity. In addition to making the solution non-physical, the aforementioned deficiency decreases the convergence rate of the SS, compared to the KP solution. Noting that the computational cost of both methods is essentially the same, it can be stated that KP supersedes SS.

9. CONCLUSION

The problem of EM diffraction from the parallel-plate multiport can be solved using the KP method without intricate mathematics. There is no need to directly be involved with the WS integrals and, thus, hypergeometric functions for the formulation of the problem. Construction of the governing linear system of equations is possible using the Fourier function space and thus, there is no need to be involved with Jacobi's polynomials. Evaluation of required improper integrals does not need complicated mathematics and can be properly carried out using standard quadrature rules and available mathematical packages. The next step can be generalization of the analysis to three dimensions.

APPENDIX A

There is no need for the direct application of the WS integrals. The following integral identities are sufficient to formulate many problems using the KP method [28].

$$\int_0^\infty J_{2m+1}(\xi)\sin\xi x d\xi = \frac{\sin\left((2m+1)\sin^{-1}x\right)}{\sqrt{1-x^2}}\Pi(2x) \tag{A1}$$

$$\int_0^\infty J_{2m}(\xi)\cos\xi x d\xi = \frac{\cos\left(2m\sin^{-1}x\right)}{\sqrt{1-x^2}}\Pi(2x) \tag{A2}$$

$$\int_0^\infty J_{2m+2}(\xi)\sin\xi x\frac{d\xi}{\xi} = \frac{\sin\left((2m+2)\sin^{-1}x\right)}{2m+2}\Pi(2x) \tag{A3}$$

$$\int_0^\infty J_{2m+1}(\xi)\cos\xi x\frac{d\xi}{\xi}=\frac{\cos\left((2m+1)\sin^{-1}x\right)}{2m+1}\Pi(2x) \tag{A4}$$

wherein m = 0, 1, 2, … and Π stands to the rect function.

APPENDIX B

Projecting the governing continuity conditions over Fourier functional space is carried out using:

$$\int_{-\pi}^{\pi}\cos nx\cos\xi x dx=\frac{2(-1)^n\,\xi\sin\xi\pi}{\xi^2-n^2} \tag{B1}$$

$$\int_{-\pi}^{\pi}\sin\left[(2n+1)x/2\right]\sin\xi x dx=\frac{2(-1)^n\,\xi\cos\xi\pi}{\left[(2n+1)/2\right]^2-\xi^2} \tag{B2}$$

$$\int_{-\pi}^{\pi}\cos\left[(2n+1)x/2\right]\cos\xi x dx=\frac{(2n+1)(-1)^n\cos\xi\pi}{\left[(2n+1)/2\right]^2-\xi^2} \tag{B3}$$

$$\int_{-\pi}^{\pi}\sin nx\sin\xi x dx=\frac{2n(-1)^n\sin\xi\pi}{\xi^2-n^2} \tag{B4}$$

REFERENCES

[1] Kobayashi, I. "Darstellung eines Potentials in zylindrischen Koordinaten, das sich auf einer Ebene innerhalb und ausserhalb einer gewissen Kreisbegrenzung verschiedener Grenzbedingung unterwirft," *Science Reports of the Tohoku Imperial University*, Ser. I, **20** (2), pp. 197-212 (1931).

[2] Sneddon, I. N., *Mixed Boundary Value Problems in Potential Theory*. North-Holland Publishing Company, Amsterdam (1966).

[3] Hongo, K. and Serizawa, H. "Kobayashi potential in electromagnetism," *IEICE Transactions*, **E95-C** (1) (2012).

[4] _____ "Scattering from a thin rectangular plate at glancing incidence", *Electromagnetics*, **21**(2), pp. 147–163 (2001).

[5] Mittra, R. and Lee S. W., *Analytical Techniques in the Theory of Guided Waves*, The MacMillan Company (1971).

[6] Daniele, V. G. and Zich, R. S., *Wiener-Hopf Method in Electromagnetics*, SciTech Publishing, Edison, NJ (2014).

[7] Harrington, R., *Field Computation by Moment Methods*, Wiley-IEEE Press (1993).

[8] Jin, J. M., *The Finite Element Method in Electromagnetics*, 3rd ed., Wiley-IEEE Press (2014).

[9] Nomura, Y. and Katsura, S. "Diffraction of electromagnetic waves by circular plate and circular hole," *Phys. Soc. Jap*., **10**, pp. 285-304 (1955).

[10] _____, "Diffraction of electromagnetic waves by ribbon and slit," *J. Phys. Soc. Jap.*, **12**, pp. 190-200 (1957).

[11] Hongo, K. "Diffraction by a flanged parallel-plate waveguide," *Radio Sci*., **7**(10,) pp. 955–963 (1972).

[12] Hongo, K. and Ishii, G. "Diffraction of an electromagnetic plane wave by a thick slit,"' *IEEE Trans. Antennas Propag*., **26**(3), pp. 494–499 (1978).

[13] Sato, R. and Shirai, H. "Electromagnetic wave scattering by a trough on a ground --E polarization case," *Memoirs Faculty Ed. Niigata Univ*., **39**, pp. 1-9 (1997).

[14] Hongo, K. and Serizawa, H. "Diffraction of electromagnetic plane wave by a rectangular plate and a rectangular hole in the conducting plate," *IEEE Trans. Antennas Propag*., **47**(6), pp. 1029–1041 (1999).

[15] _____, "Diffraction of an acoustic plane wave by a rectangular hole in an infinitely large rigid screen," *J. Acoust. Soc. Amer*., **106**(1), pp. 29–35 (1999).

[16] Hongo, K. and Serizawa, H. "Radiation from a flanged rectangular waveguide," *IEEE Trans. Antennas Propag*., **53**(12), pp. 3953-62 (2005).

[17] Imran, A. Naqvi, Q. and K. Hongo, "Diffraction of electromagnetic plane wave by an impedance strip," *PIER*, **75**, pp. 303–318 (2007).

[18] Ghalamkari, B. Tavakoli, A. and Dehmollaian, M. "A Fast Semianalytical Solution of a 2-D Dielectric-Filled and Coated Rectangular Groove," *IEEE Trans. Antennas Propag*., **62**(10), pp. 5099–5107 (2014).

[19] Qadeer, N. Bhatti, N. Naqvi, Q. A. *et al*. "Use of Kobayashi potential method and Lorentz–Drude model to study scattering from a PEC strip buried below a lossy dispersive NID dielectric-magnetic slab", *Appl. Math. Comput*., **362**, pp.124573 (2019).

[20] Javed, S. F. Abbas, M. and Naqvi, Q. A. "Scattering from a PEC strip buried in non-integer dimensional planar grounded dielectric slab by using Kobayashi potential method", *Physics Letters A* (2019).

[21] Davoudabadifarahani, H. and Ghalamkari, B. "Analytical solution of electromagnetic scattering by PEMC strip embedded in chiral medium*", Eng. Anal. Bound. Elem*., **113**, pp.1 (2020).

[22] Shaukat, H. Shoukat, S. and Naqvi,Q. A. "Plane-wave electromagnetic scattering from a PEC strip placed at the interface of non-integer dimensional spaces", *Optik*, **218**, pp. 165007 (2020).

[23] Davoudabadifarahani, H. and Ghalamkari, B. "Rigorous electromagnetic scattering solution of a PEMC strip placed at interface of dielectric-chiral media using Kobayashi potential", *Waves Random Complex Media*, pp.1 (2020).

[24] Barati, P. and Ghalamkari, B. "Semi-analytical solution of electromagnetic wave scattering from PEC strip located at the interface of dielectric-TI media", *Eng. Anal. Bound. Elem*., **123**, pp. 62 (2021).

[25] Barati, P. and Ghalamkari, B. "Semi-analytical solution of electromagnetic scattering of a slit in PEC plane located in TI medium*", Eng. Anal. Bound. Elem*, **128**, pp. 35 (2021).

[26] _____ "Electromagnetic scattering of the PEMC strip located at the interface of topological insulator-dielectric by utilizing Kobayashi potential method", *Eng. Anal. Bound. Elem*., **135,** pp. 258 (2022).

[27] Davoudabadifarahani, H. and Ghalamkari, B. “Rigorous EM Scattering Solution from a Slit in an IBC Plate with Different Surface Impedances Placed Between Two Different Chiral Media”, *IEEE Trans. Antennas Propag*., **70**(11), pp. 10843–50 (2022).

[28] Gradshteyn, I. S. and Ryzhik, I. M. *Table of Integrals, Series, and Products,* 8th ed*.,* Elsevier Academic Press (2015).

[29] Honarbakhsh, B. “Comment on “Diffraction by a Flanged Parallel-Plate Waveguide””, *Radio Science*, 57(8) (2022).

[30] Abramowitz, M. and Stegun, I. *Handbook of Mathematical Functions with Formulas, Graphs, and Mathematical Tables*. Dover, New York (1964).

[31] Myint U, T. and Debnath, L*. Linear Partial. Differential Equations for Scientists and Engineers,* 4th ed., Birkhäuser (2007).

[32] Rautio, J. C. “The microwave point of view on software validation", *IEEE Antennas Propag. Mag.*, **38**(2), pp. 68-71 (1996).

[33] Van Bladel, J. *Singular Electromagnetic Fields and Sources,* IEEE Press (1991).

[34] Marcuvitz, N. *Waveguide Handbook*, McGraw-Hill (1951).

[35] Park, K.H. Eom, H.J. and Yamaguchi, Y. “An analytic series solution for E-plane T-junction in parallel-plate waveguide,” *IEEE Trans. Microw. Theory Tech*., **42**(2) (1994).

[36] Park, K. H. and Eom, H. J. “An Analytic Series Solution for H-Plane Waveguide T-Junction,” *IEEE Microw. Guided Wave Lett.*, **3**(4), pp. 104-106 (1993).

[37] Cho, Y. H. “New iterative equations for an E-plane T junction in a parallel plate waveguide using Green’s function,” *Microw. Opt. Technol. Lett.*, **37**, (2003).

[38] Cho, Y. H. “Iterative Green’s function analysis of an H-plane T-junction in a parallel-plate waveguide,” *J. Electromagn. Waves Appl.*, **18**(9), pp. 1195–1202 (2004).

[39] Veronis, G. and Fan, S. “Bends and splitters in metal-dielectric-metal subwavelength plasmonic waveguides,” *Appl. Phys. Lett*. **87**, (2005).

[40] Pozar, D. M. *Microwave Engineering*, 4th ed., Wiley (2011).

Fig. 1. Cross section of the parallel-plate multiport.

Fig. 2. Convergence analysis.

Fig. 3. Singular fields over the T-junction: (a) $\mathbf{H}_x^{TE}\left(A/m\right)\big|_{y=0}$, (b) $\mathbf{E}_x^{TM}\left(V/m\right)\big|_{y=0}$.

Fig. 4. Singular fields over the X-junction: (a) $\mathbf{H}_x^{TE}\left(A/m\right)\big|_{y=0}$, (b) $\mathbf{H}_x^{TE}\left(A/m\right)\big|_{y=d}$, (c) $\mathbf{E}_x^{TM}\left(V/m\right)\big|_{y=0}$, (d) $\mathbf{E}_x^{TM}\left(V/m\right)\big|_{y=d}$.

Fig. 5. TE field over the cross section for the T-junction: (a) $\left|E_z^{TE}\right|$ (normalized), (b) $\arg E_z^{TE}\left(\text{rad}\right)$.

Fig. 6. TE field over the cross section for the X-junction: (a) $\left|E_z^{TE}\right|$ (normalized), (b) $\arg E_z^{TE}\left(\text{rad}\right)$.

Fig. 7. TM field the cross section for the T-junction: (a) $\left|H_z^{TM}\right|$ (normalized), (b) $\arg H_z^{TM}\left(\text{rad}\right)$.

Fig. 8. TM field the cross section for the X-junction: (a) $\left|H_z^{TM}\right|$ (normalized), (b) $\arg H_z^{TM}\left(\text{rad}\right)$.

Fig. 9. Power ratios vs. width of the horizontal section for the X-junction at TM incidence wherein P_i (P_r) represents the incident(reflected) power at $y=0$, and P_t represents the transmitted power at $y=d$.

Fig. 10. Performance of the KP method for different junction size assuming TM polarization: (a) convergence, (b) computational cost in logarithmic scale.

Fig. 11. Asymptotic analysis for the TE case for: (a) $d\to 0$ with $\mu_1=\mu_2=\mu_0$, (b) $d\to\infty$ with $\mu_1=\mu_0$ and $\mu_2=\left(1-j0.001\right)\mu_0$.

Fig. 12. KP vs. SS for TE polarization: (a) aperture electric field, (b) aperture magnetic field, (c) convergence, (d) computational cost.

Fig. 13 KP vs. SS for TM polarization: (a) junction electric field, (b) junction magnetic field, (c) convergence curve, (d) computational cost.

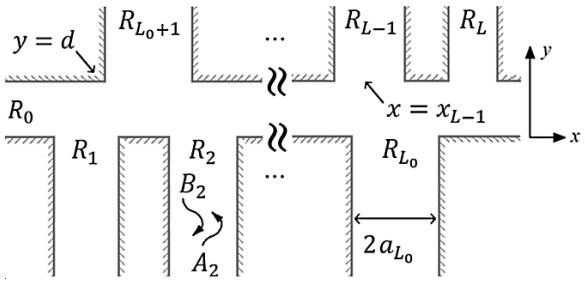

Fig. 1.

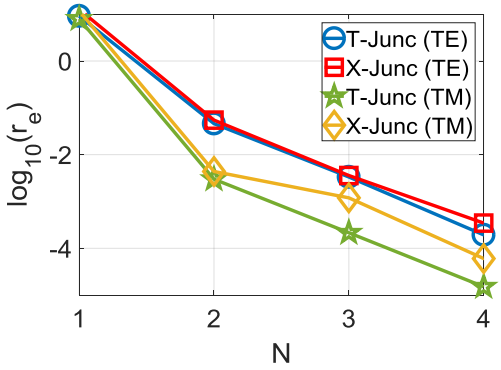

Fig. 2.

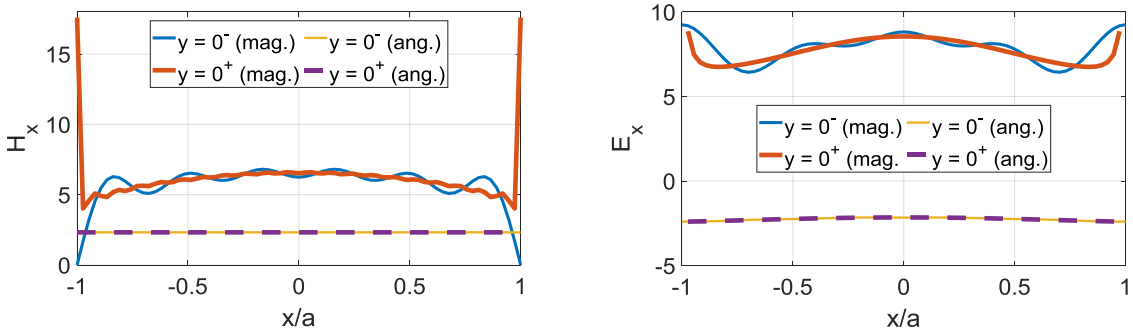

(a) (b)

Fig. 3.

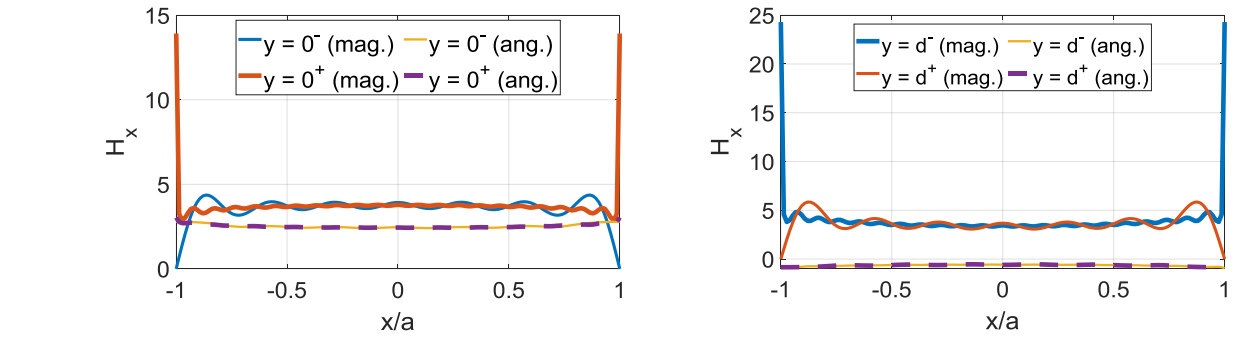

(a) (b)

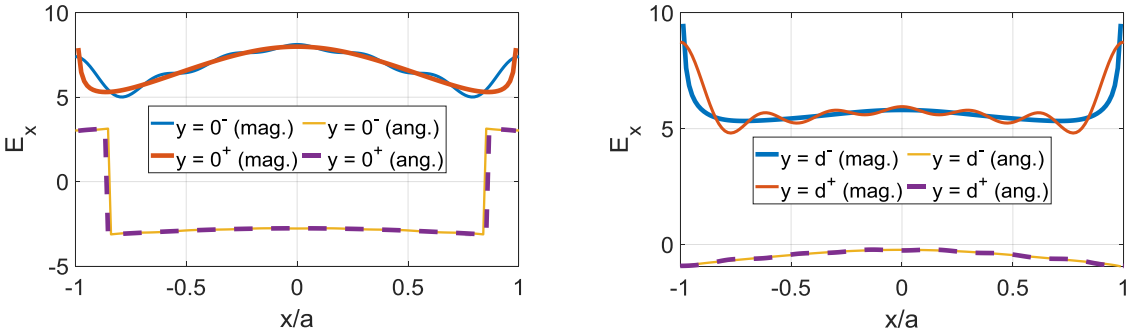

(c) (d)

Fig. 4.

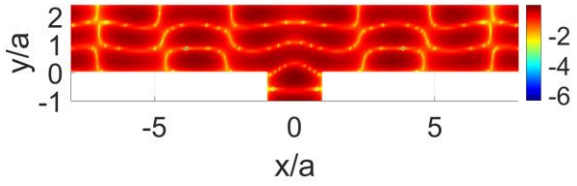

(a)

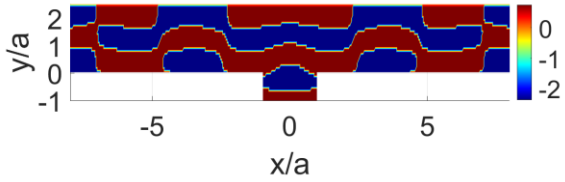

(b)

Fig. 5.

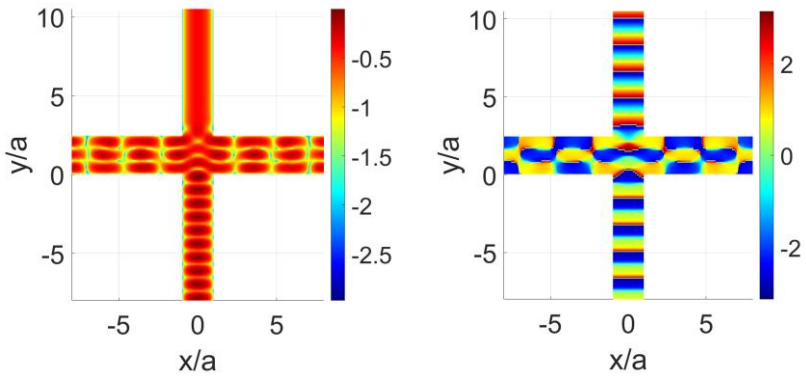

(a) (b)

Fig. 6.

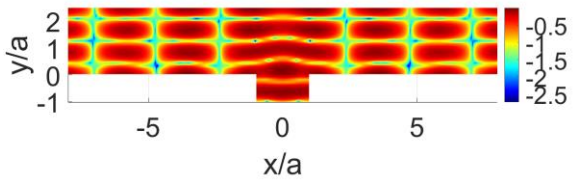

(a)

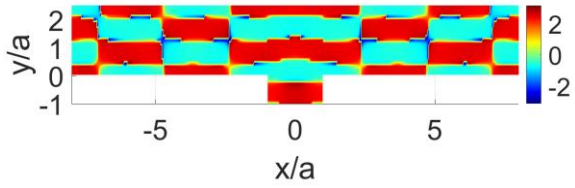

(b)

Fig. 7.

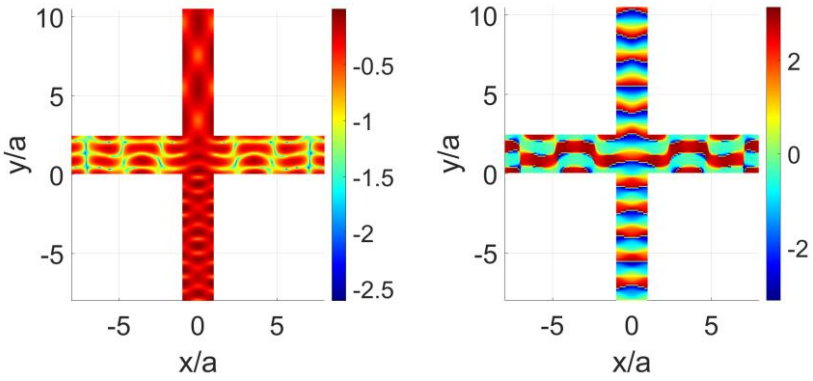

(a) (b)

Fig. 8.

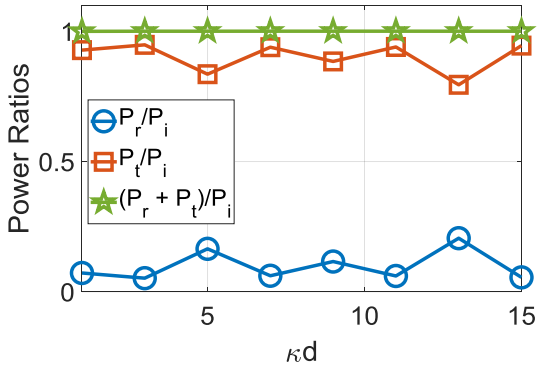

Fig. 9.

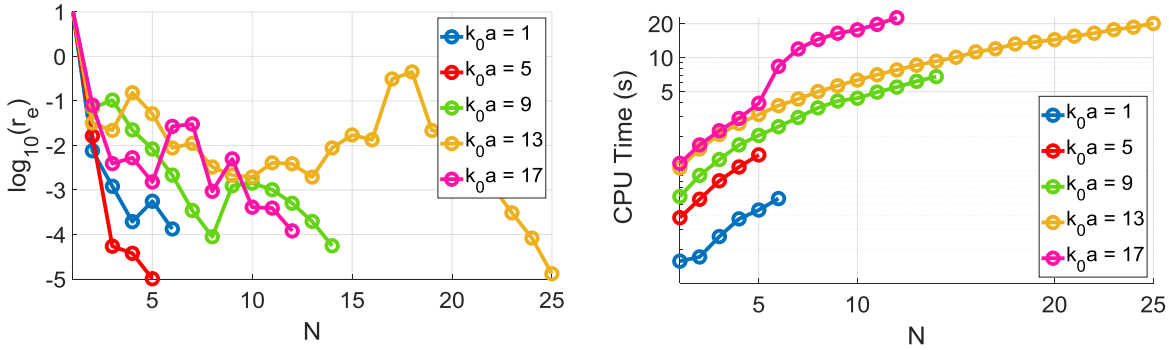

(a) (b)

Fig. 10.

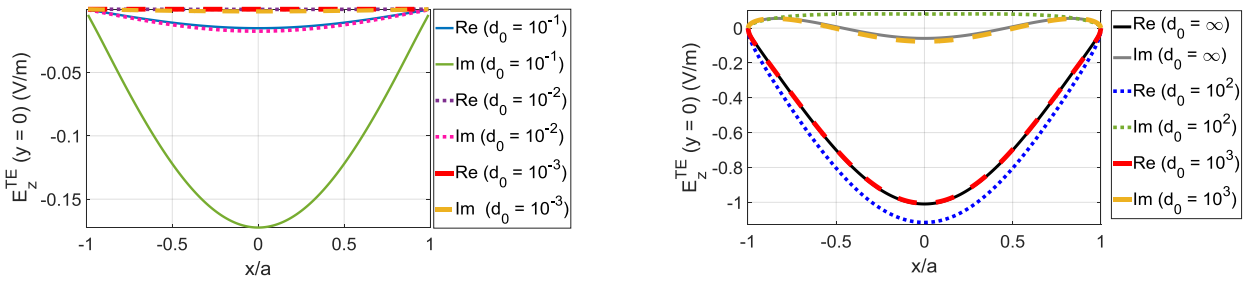

(a) (b)

Fig. 11.

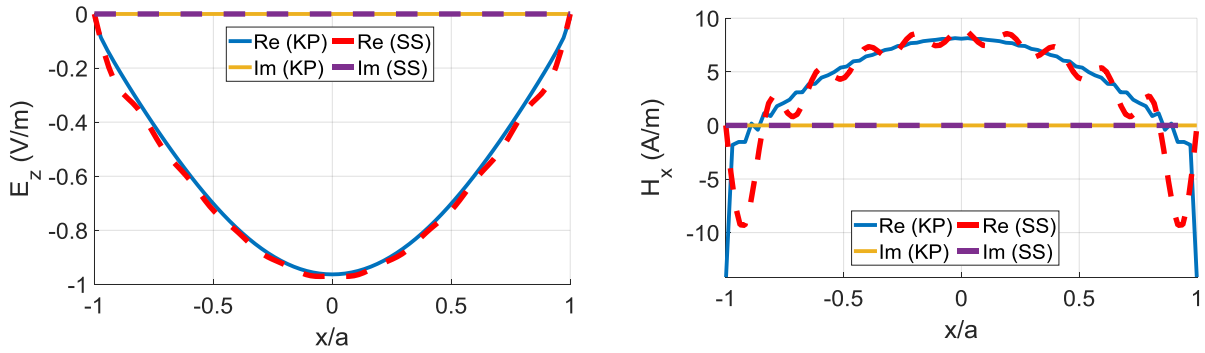

(a) (b)

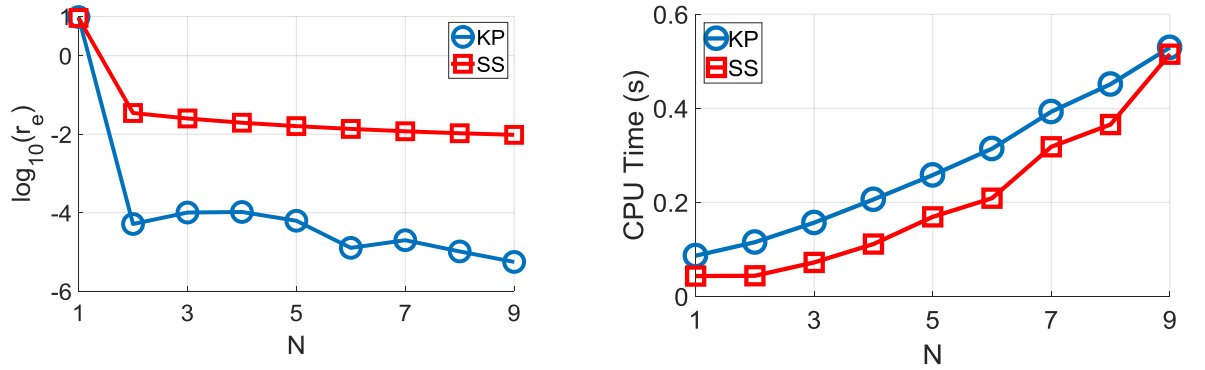

(c) (d)

Fig. 12 .

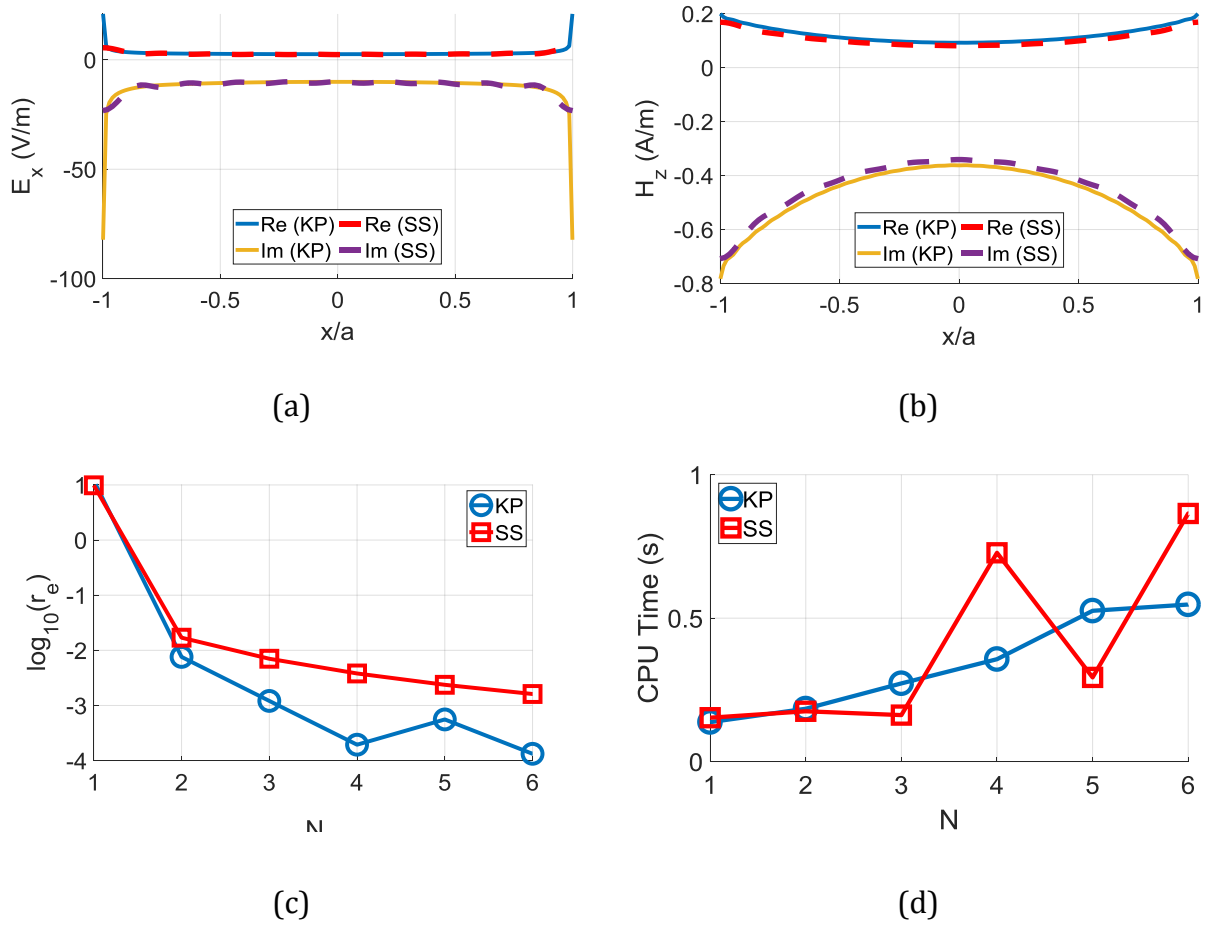

Fig. 13.

Babak Honarbakhsh was born in Tehran, Iran, in 1981. He received his B.S., M.S. and Ph.D. degrees in electrical engineering, all from Amirkabir University of Technology (Tehran Polytechnic), in 2004, 2007 and 2012. He is currently an Assistant Professor in the Department of Electrical Engineering at Shahid Beheshti University. His research interest is electromagnetic theory and numerical electromagnetics.